

Abstract. Nanocomposite strain sensors have shown application prospect in a wide range of applications. However, the sensitivities of the existing nanocomposite strain sensors to high-frequency dynamic strains are rather unsatisfactory. Herein, we fabricate a highly sensitive nanocomposite sensor for acquiring microscopic vibrations generated by ultrasonic waves, from polydopamine(PDA)-coated hybrid carbon nanofillers. First, multi-walled carbon nanotubes (MWCNTs) are coated by 10s nm thick viscous PDA to improve their compatibility with polyvinylidene fluoride substrates. Compared to uncoated MWCNTs, the use of 15 wt.% PDA-coated MWCNTs leads to a 40% increase in sensitivity. Then, one-dimensional PDA@MWCNTs are mixed with two-dimensional single-layer graphene to enhance the geometric contact between nanofillers. The sensitivity of sensors with hybrid nanofillers far exceeds that of PDA@MWCNTs sensors. Also, as the mass fraction of graphene within hybrid nanofillers expands from 33% to 66%, the sensitivity of the proposed sensor improves by approximately 120%, surpassing that of pure graphene sensors. The high sensitivity of the proposed sensor, which actually utilizes a lower graphene content, was shown to be derived from the synergy between the two types of nanofillers which are of different dimensionalities. This study presents a novel approach for optimizing the sensitivity of nanocomposite strain sensors to high-frequency micro-vibrations.

1. Introduction

Sensors with significant sensitivities to small deformations have become considerably crucial to a number of high-value-added applications such as wearable electronics^{1,2}, human machine interface^{3,4}, and condition monitoring of high-stake engineering structures^{5,6}. The development of advanced materials such as low-dimensional nanomaterials has given rise to sensors that are more powerful, multifunctional and intelligent⁷⁻¹⁰. By exploiting the advantages of nanomaterials¹¹⁻¹⁴, nanocomposite strain sensors that are light, physically flexible, and more sensitive than conventional strain sensors, capable of detecting even smaller deformations,

have been introduced. In particular, by optimizing synthesis processes, it is possible to fabricate nanocomposite strain sensors that can be used to probe high-frequency microscopic vibrations, e.g. those that are generated by ultrasonic waves¹⁵⁻¹⁶ which constitute one of the most widely used categories of diagnostic means for *in situ* assessments of structural integrity¹⁷⁻¹⁸.

The tunneling effect^{19, 20} and the piezoresistive effect^{21, 22} are the main physical principles that enable nanocomposite strain sensors to capture ultrasound waves. When a nanocomposite strain sensor is impinged by the dynamic strains generated by ultrasonic waves, the conductive nanofillers inside the material will be vibrated at the microscopic level. Such micro-vibrations will induce two microscopic phenomena: (i) the dimensions of the nanofillers will change, causing the intrinsic electrical resistances of the nanofillers to vary due to the piezoresistive effect, and (ii) the distances between adjacent nanofillers will fluctuate, triggering the tunneling resistances across the nanofillers to oscillate due to the tunneling effect. As a result, a microscopic change in the overall electrical resistance of the sensor will be induced. Therefore, the key to designing nanocomposite strain sensors for acquiring ultrasonic waves essentially lies on how to effectively convert high-frequency micro-vibrations into changes in electrical resistance.

Carbon nanofillers such as carbon black (CB) and carbon nanotubes (CNTs) have shown application prospects in capturing ultrasonic waves^{13, 23, 24}. Compared with traditional strain sensors, nanocomposite strain sensors possess higher sensitivities, especially when the nanofiller content of a sensor is close to the percolation threshold of the material used^{25, 26}. At the percolation threshold, the nonlinear change in the electrical resistance of a nanocomposite strain sensor has been shown numerically and experimentally to be related to the tunneling effect. Under micro-vibrations, the change in the electrical resistance of the sensor would be mainly determined by the tunneling effect between adjacent nanofillers, as opposed to the splitting of the conductive network²⁷.

In fact, the sensitivities of the existing nanocomposite strain sensors to ultrasonic waves are far from satisfactory²⁸⁻³⁰. This in turn has been preventing these sensors from realizing real-world applications in the ultrasonic regime. There may be two main reasons³¹⁻³³ behind the limited sensitivities of the existing sensors. One is that the agglomeration of nanofillers^{34, 35} or the unfavorable capacitive compatibility between nanofillers and polymer matrices^{36, 37} would result in adversely dispersed nanofillers inside nanocomposite structures. The other is the lack of effective tunneling nodes^{38, 39} inside nanocomposite structures which would render the micro-vibrations that are generated by ultrasonic waves less evident through changes in the electrical resistances of sensors.

The tunneling resistance⁴⁰ plays the pivotal role in determining changes in the electrical resistances of nanocomposite strain sensors that are subjected to micro-vibrations. For instance, the tunneling resistance (R_t) between two carbon nanofillers can be approximated by Simmons'

theory¹ as $R_t = \frac{V}{AJ} = \frac{h^2 d}{\sqrt{2m\lambda} A e^2} \exp\left(\frac{4\pi d}{h} \sqrt{2m\lambda}\right)$, where V is the potential difference, A is the cross-sectional area of the tunneling junction, J is the tunneling current density, h is the Planck's constant, d is the distance between the two nanofillers, m is the mass of electron, e is the quantum of electron, and λ is the barrier height of the substrate. The formula essentially describes that the tunneling resistance of a sensor is positively related to the cut-off tunneling distance (d) of the sensor. Normally, the cut-off tunneling distance of a sensor depends on several factors, such as the type of the nanofillers, the type of the insulating substrate, and the processing method. Moreover, the cut-off tunneling distance is in the range of a few to 10s of nanometers. For example, the cut-off tunneling distance between two parallel graphene sheets in a polymer substrate was found to be a few to a dozen of nanometers⁴¹⁻⁴³. The cut-off distances of the AgNW-PDMS-AgNW and the CNT-polymer-CNT channels have been reported^{22, 44, 45} to be approximately 0.58 nm and 1-1.8 nm, respectively. Therefore, a method to effectively control the dispersion distances between nanofillers, such as coating a nanolayer

like PDA, would have a positive impact on the sensitivity of nanocomposite strain sensors to micro-vibrations.

It has been reported that the electrical and the mechanical properties of a nanocomposite strain sensor are directly influenced by the dimensionalities of the carbon nanofillers that are used⁴⁶. Zheng et al. fabricated a CNT/CB nanocomposite sensor which exhibits a high stretchability, a strain-dependent sensitivity over a wide range of strain (ca. 300% strain), and an excellent linear current-voltage behavior⁴⁷. Mixing of nanofillers of different dimensionalities enhances the boundary geometric contact between nanofillers at the microscale, leading to more significant changes in the tunneling resistances of nanocomposite strain sensors under micro-vibrations. A hybrid CNT/graphene based nanocomposite material contains many CNTs and graphene flakes that are tangled and folded in a complex network inside the polymer matrix⁴⁸. When an external tensile strain is applied, the deployment of the tangled elastic nanofillers is more likely to slide in the axial direction, thereby changing the electrical resistance of the material. The geometric effect that is induced by the stacking of the hybrid nanofillers increases the number of tunneling nodes at the nanoscale⁴⁹. This shows that hybrid carbon nanofillers^{43, 50-52} would have also improve the sensitivity of nanocomposite strain sensors to the micro-vibrations that are generated by ultrasound waves.

Based on the above analysis, we propose a new nanostructure to increase the sensitivity of nanocomposite strain sensors to ultrasonic waves. First, the surfaces of multi-walled carbon nanotubes (MWCNTs) are deposited by *in situ* polymerization of dopamine (DA). The polydopamine(PDA)-coated MWCNTs are then mixed with single-layer graphene to form a precursor. The precursor is further mixed with polyvinylidene fluoride (PVDF). Finally, hybrid PDA@MWCNT/graphene nanocomposite strain sensors are fabricated by blade coating. The PDA coating on the MWCNTs, which has a large viscosity, does not only act as a dispersed phase that reduces the entanglement of MWCNTs, but also serves as the buffer layers between

the MWCNTs and the PVDF matrices, helping to improve the responsiveness of the sensors to high-frequency micro-vibrations. On the other hand, the mixing of one- and two-dimensional nanofillers can effectively increase the number of tunneling nodes within a unit volume in the nanostructure, compared with the use of nanofillers of a single dimensionality. By examining the amplitudes of the ultrasonic signals that were received by the sensors, it was found that the new nanostructure brings forward a significant improvement in the sensitivity to the micro-vibrations that are generated by ultrasonic waves.

2. Experimental

2.1. Materials

MWCNTs (inner diameter: 5-10 nm, outer diameter: 10-20 nm, length: 10-30 μm), graphene (thickness: 4-7 nm, diameter: 6 μm , purity: 99.7%) and dopamine were supplied by Shanghai Aladdin Bio-Chem Co., Ltd., China. Tris-HCl buffer (pH: 8.5) and PVDF were purchased from Nantong Xingchen Synthetic Materials Co., Ltd., China. 1H,1H,2H,2H perfluorodecyl trichlorosilane (volume fraction: 0.025%) and N, N-Dimethylformamide (DMF) were provided by Tianjin Damao Chemical Reagent Factory, China.

2.2. Preparation of nanocomposite sensors

2.2.1. Synthesis of PDA@MWCNTs

0.06-0.15 g of dopamine was dispersed in 30 mL of Tri-HCl buffer (pH: 8.5), and 0.1 g of MWCNTs were then added. The reaction was performed at 25 $^{\circ}\text{C}$ for 12 hours. The product of the reaction was washed with distilled water 3 to 5 times, dried, immersed in 20 mL of n-hexane solution containing 1H,1H,2H,2H perfluorodecyl trichlorosilane (volume fraction: 0.025%), washed with absolute ethanol 3 times, and dried at 60 $^{\circ}\text{C}$ for 2 hours. The solid PDA@MWCNTs that were obtained were placed in a dry box overnight to remove excess water.

2.2.2. Fabrication of nanocomposite sensors

Carbon nanofillers and PVDF were put into 10 mL of DMF solution. The nanocomposite solution was mechanically stirred at 30 °C for 4 hours to ensure thorough mixing. A polyimide (PI) film was fixed on a table and flattened by a vacuum pump. A 20 mm × 10 mm mold was placed on the PI film. The nanocomposite solution was dropped on the PI film within the mold and scraped back and forth by a blade which was positioned at a constant height of 50 μm. During this process, the temperature of the table was maintained at 25 °C. Once the volatile solvent in the nanocomposite solution had evaporated, a nanocomposite sensor film with a thickness of 50 μm was obtained as shown in **Fig. 1(a)**. The film was then cut into individual sensors of desired dimensions. The manufacturing process is simple and efficient and leads to sensors with uniform thicknesses.

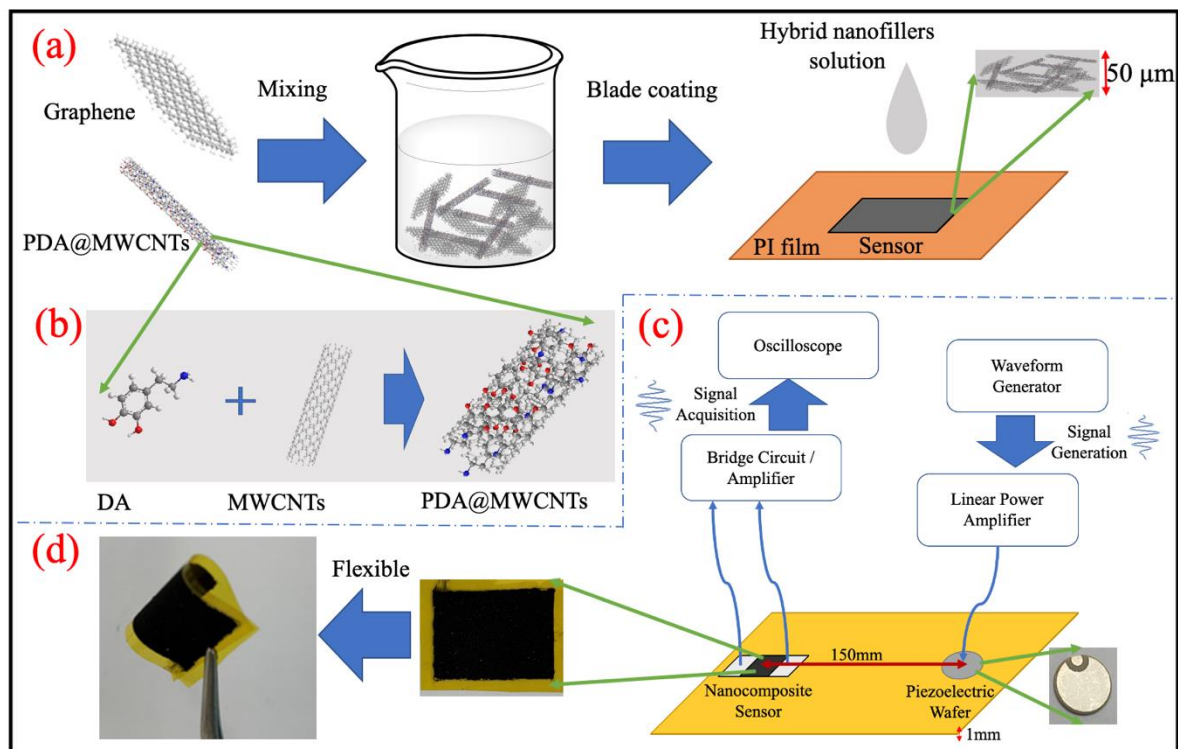


Figure 1. (a) The fabrication procedure of the proposed nanocomposite sensor with hybrid nanofillers. (b) *In situ* polymerization of DA on the surfaces of MWCNTs. (c) Measurement

of the responses of nanocomposite sensors to ultrasonic waves. (d) A typical flexible nanocomposite sensor.

In this work, three sets of nanocomposite sensors were fabricated at the same nanofiller content of 15 wt.%. The first set consists of a sensor that was made from uncoated MWCNTs only, and a couple of other sensors that were made by coating MWCNTs with PDA at mass fractions of 10% and 15% (labelled as PDA10%@MWCNT and PDA15%@MWCNT). For the second set of sensors, graphene was mixed with uncoated MWCNTs, PDA10%@MWCNT or PDA15%@MWCNT at a mass ratio of 1:1 to form hybrid nanofillers (labelled as Gra/MWCNT, Gra/PDA10%@MWCNT and Gra/PDA15%@MWCNT). The third set consists of a pure graphene sensor, and three other sensors that were made by mixing graphene and PDA15%@MWCNT at mass ratios of 1:2, 1:1 and 2:1 (labelled as $m_{\text{Gra}}/m_{\text{PDA15\%@MWCNT}}=1:2$, $m_{\text{Gra}}/m_{\text{PDA15\%@MWCNT}}=1:1$ and $m_{\text{Gra}}/m_{\text{PDA15\%@MWCNT}}=2:1$).

2.3. Material characterization

Scanning electron microscopy (SEM). The microscopic morphologies of nanocomposite sensors were observed using a Hitachi S3400N Scanning Electron Microscope (Japan).

Transmission electron microscopy (TEM). TEM was performed using a JOEL JEM-1230 Transmission Electron Microscope (USA).

X-ray photoelectron spectroscopy (XPS). XPS was conducted using a Thermo Scientific K-Alpha Spectrometer System (USA) that is equipped with a monochromatic Al K α X-ray source (1486.6 eV) operating at 100 W. Samples were analyzed under vacuum ($P < 10^{-8}$ mbar) with a pass energy of 150 eV (survey scans) or 25eV (high-resolution scans). All peaks were calibrated against the C1s peak for adventitious carbon which has a binding energy of 284.8 eV. The experimental peaks were fitted by the Thermo Scientific Avantage Software.

X-ray diffraction analysis (XRD). XRD was performed using a Rigaku D/MAX-3C X-ray Diffractometer (Japan) with Cu K α radiation. Samples were scanned at a speed of 10°/min under the diffraction angle 2θ in the range of 5–90°.

Raman spectroscopy. Laser Raman spectroscopy was performed using a Renishaw inVia Confocal Raman Microscope (UK) excited at 632.8 nm with a NeHe laser (17 mW). Samples were scanned in the range of 100–4000 cm⁻¹ for 5–20 times.

2.4. Measurement of responses of nanocomposite sensors to ultrasonic waves

The experimental setup that was used to examine the sensitivities of nanocomposite sensors to the micro-vibrations that are generated by ultrasonic waves is shown in **Fig. 1(c)**. For each experiment, a nanocomposite sensor and a piezoelectric wafer were glued on a 1 mm thick glass fiber reinforced polymer (GFRP) panel, separated by a distance of 150 mm. On the nanocomposite sensor, a pair of electrodes were establishing using silver paste, and wires were attached to the electrodes. A waveform generator (PXI-5412, National Instruments, USA) was used to generate a 5-cycle Hanning-windowed sinusoidal toneburst, and the signal was amplified by a linear amplifier (US-TXP-3, Ciprian, France) before it was used to excite the piezoelectric wafer. The ultrasonic waves that were generated by the piezoelectric wafer propagated along the GFRP panel and impinged the nanocomposite sensor, causing it to undergo micro-vibrations that are not visible to the naked eyes. **The micro-vibrations would have caused the dimensions of the nanofillers in the sensor to change and the distances between adjacent nanofillers to fluctuate. While the former phenomenon would have varied the intrinsic electric resistances of the nanofillers, the latter would have oscillated the tunnelling resistances across adjacent nanofillers. The end result was a microscopic change in the overall electrical resistance of the sensor.** The change in electrical resistance was then converted by an inhouse bridge circuit / amplifier unit⁵³ into an electrical voltage signal which can be visualized on an oscilloscope (DSO 9064A, Agilent Technologies, Inc., USA). Due to the embedded noise of

the instruments used and the ambient noise that came from the surrounding environment, a Fourier transform based bandpass filter was used to eliminate the noise in the signals received.

The inhouse bridge circuit / amplifier unit consists of a voltage divider, a capacitor and an amplifier. The unit was supplied with a 10 VDC. During an ultrasonic experiment, the electrical resistance of the voltage divider would need be adjusted to be balanced with the base electrical resistance of the nanocomposite sensor used. When the sensor was impinged by the dynamic strain induced by ultrasonic waves, the electrical resistance of the sensor would change. The capacitor would cancel out the static voltage in the circuit so that the output electrical voltage signal would only reflect the electrical resistance change of the sensor.

3. Results and discussion

3.1.Characterization of PDA@MWCNT nanocomposite sensors

Since Phillip B. Messersmith⁵⁴ and others^{55,56} carried out the first synthesis of multifunctional PDA adhesive coating that was inspired by the mussel foot silk protein, PDA has attracted widespread research interest. Related research has found that PDA can deposit on inorganic substrates, including various types of nanomaterials, as uniform coating layers, and can be further functionalized. The polymerization and cross-linking reactions of PDA can be carried out slowly and spontaneously under weakly alkaline conditions (pH: 8.5). This phenomenon can be well explained by the equilibrium movement mechanism proposed by the predecessors, which embodies a series of reactions, including a step for forming an indole structure through a 3,4-dihydroxyphenylalanine cyclization reaction.

Fig. 2(a)-(c) shows the SEM images of uncoated MWCNTs. It can be seen that pure MWCNTs exhibit a long rod-like shape with a smooth surface and a rigid crystal structure. The length of a MWCNT is generally 10s μm while its radius is between 300 nm and 500 nm. Normally MWCNTs are prone to aggregation because there are not many functional groups on

their surfaces which can prevent aggregation from happening. Due to their rigid rod-like structures, MWCNTs can only give rise to weak piezoresistive effect when subjected to external strains. In this study, our goal is to increase the rates of change of the tunneling resistances of nanocomposite materials in response to micro-vibrations, as opposed to simply improving the conductive properties of the materials. However, disorganized and entangled MWCNTs are not conducive to the occurrence of the tunneling effect. Therefore, nanocomposite sensors that are made of MWCNTs generally possess weak sensitivities to ultrasonic signals (the result is presented in **Fig. 4**).

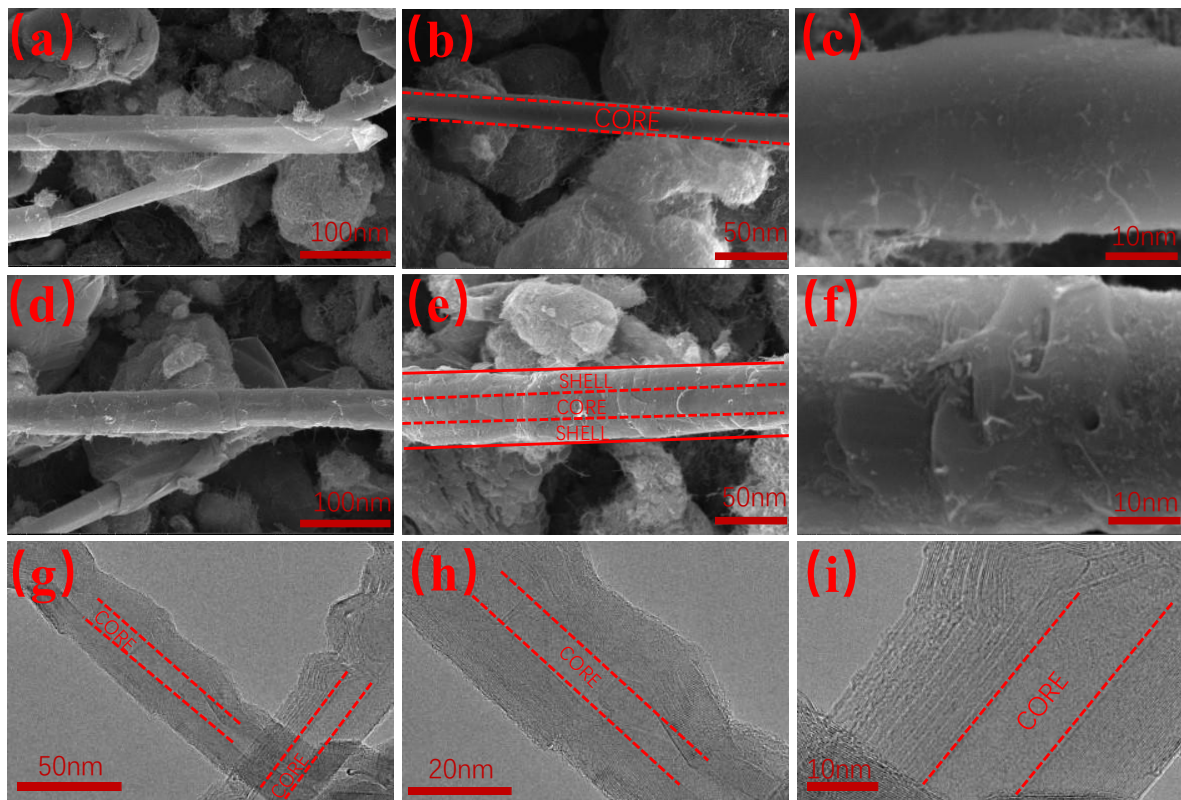


Figure 2. The SEM images of (a)-(c) uncoated MWCNTs and (d)-(f) PDA15@MWCNTs at different magnifications; (g)-(i) The TEM images of PDA15@MWCNTs at different magnifications.

Due to the insolubility of MWCNTs, the compatibility between MWCNTs and polymer matrices is poor. Also, the content of functional groups on the surfaces of MWCNTs is low.

These, together, would result in weak interfacial bonds between MWCNTs and substrates in nanocomposite strain sensors, hindering the effective transmission of external strains to nanofillers. In this work, PDA was coated on MWCNTs in order to improve the compatibility and the interfacial adhesion between MWCNTs and substrates. Since the polymer chains of PDA are highly similar to polymer substrates, they would allow MWCNTs to covalently graft to substrates, in turn improving the compatibility of MWCNTs in substrates and enhancing the adhesion of MWCNTs to substrates. Since synthesized PDA is insoluble in solvents, it would precipitate on the surfaces of MWCNTs through physical binding. As seen from the **Fig. 2 (d)-(f)**, after PDA coating had been done, the MWCNTs became rough with their surfaces exhibiting a layered structure, and the diameters of the MWCNTs increased by 10s nm. The amount of increase depended on the temperature of the reaction, the stirring speed, and the concentration of PDA. **From Fig. 2 (g)-(i), it is observed that PDA formed a layered crystalline structure covering the surfaces of the MWCNTs, and the thicknesses of the PDA layers are stably between 10 nm and 20 nm. Because of the strong viscosity of PDA, the MWCNTs and the PDA crystals were well integrated.** The PDA coating would function as buffer layers between the conductive nanofillers and the PVDF substrates, allowing high-frequency micro-vibrations that are induced by ultrasonic waves to appear as elastic vibrations as opposed to rigid vibrations.

In order to determine the crystal structures of PDA@MWCNTs, XRD pattern were obtained. As observed from **Fig. 3(a)**, the addition of PDA did not give rise to new crystalline peaks, and this confirms that no residual PDA in PDA@MWCNTs existed as a single phase. It further illustrates that strong physical bonds were formed between PDA and MWCNTs, due to the strong viscosity of PDA. In the XRD patterns, the strongest crystalline diffraction peaks appear at 26.6° , which corresponds to the faces (002), echoing with the rod-shaped graphitized MWCNT crystals. The spurious peaks, which arose from the entanglement between MWCNTs,

did not change with PDA content, indicating that the dispersion of MWCNTs remained the same with the addition of PDA. It is inferable from the small number of impurity peaks and the stronger graphite peak that the purities and the degrees of perfection of the nanocomposite materials are high.

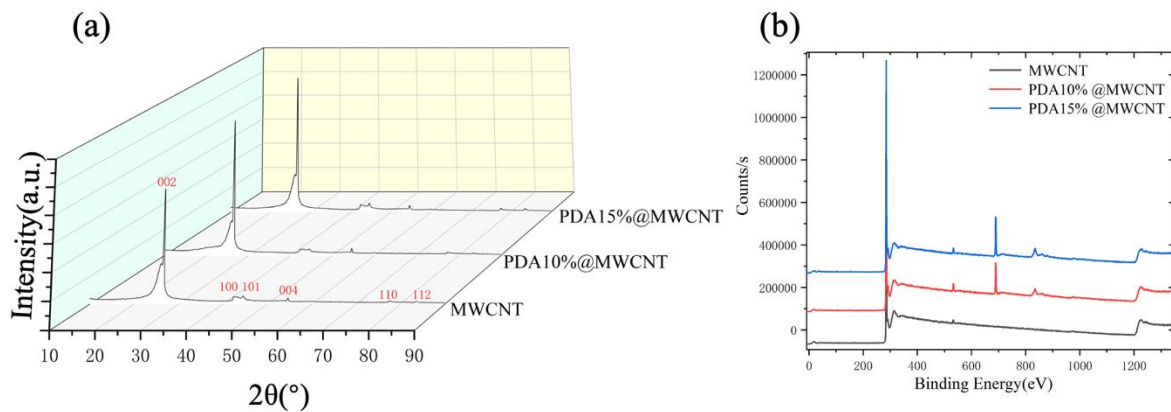


Figure 3. (a) The XRD patterns and (b) the XPS patterns of uncoated MWCNTs and PDA@MWCNTs.

Moreover, by using the JADE software, the crystallization information of the nanocomposite materials at 26.6° was obtained as shown in **Table 1**. As the amount of PDA used in the reaction was increased, the average grain size of PDA@MWCNTs also increased from 32.6 nm to 44.4 nm, in line with the increase in the amplitude of the graphite peak in the XRD patterns. This means that PDA formed a perfect crystalline phase which existed on the surfaces of crystallized MWCNTs. The increase in the grain size of PDA was attributed to the thickening of PDA coating. Together with the SEM images, we can conclude that relatively pure PDA@MWCNTs were obtained and PDA coating was very well done. The effect of PDA coating was evident through the difference between the ultrasonic signals that were acquired by nanocomposite sensors with uncoated MWCNTs and with PDA@MWCNTs (the result is presented in **Fig. 4**).

Table 1. The crystallization information of uncoated MWCNTs and PDA@MWCNTs.

	$2\theta(^{\circ})$	Crystal plane distance(nm)	Average grain size(nm)
Uncoated MWCNT	26.668	3.3399	32.6
PDA10%@MWCNT	26.607	3.3474	43.2
PDA15%@MWCNT	26.645	3.3551	44.4

In order to obtain further information of the pad surface, surface analysis of the nanocomposite sensors was carried out using XPS. As shown in Fig. 2(b), the additional peaks at 697.5 eV and 846.3 eV for the PDA@MWCNTs samples confirm the existence of PDA. These peaks did not change with PDA content, meaning that the chemical environments of PDA10%@MWCNT and PDA15%@MWCNT were the same. The XPS spectra of the C1s, O1s, C (KLL), O (KLL) and Ns peaks are shown in Fig. S1. The fact that the addition of PDA did not give rise to new carbon peaks, as seen in the XPS survey spectra in Fig. 2(b), and did not shift the C1s peak, as seen in the XPS spectra of C1s in Fig. S1 (c), (f) and (i), demonstrates that the surfaces of MWCNTs retained the same chemical environment and that the binding between PDA layers and MWCNTs was physical. The O1s and N1s peaks did not shift with PDA content, illustrating that the energy levels of these elements remained stable. On the other hand, the O1s peak became higher and broader with an increase in PDA content. This does not only mean that PDA was perfectly coated, but also shows that the PDA was evenly dispersed on the surfaces of MWCNTs.

3.2. Performances of PDA@MWCNTs nanocomposite sensors in acquiring ultrasonic waves

The first diagram in Fig. 4(a) shows the excitation signal that was used, which is a 5-cycle Hanning-windowed sinusoidal toneburst with a central frequency of 100 kHz. It can be seen from the subsequent diagrams that the nanocomposite sensors are able to capture the two modes

of ultrasonic waves that propagate in plate-like structures, i.e. the fundamental symmetric Lamb wave mode (denoted by S_0) and the fundamental anti-symmetric Lamb wave mode (denoted by A_0). It was discussed earlier that the thickness of the cladding layer on the surfaces of MWCNTs increased with the amount of PDA that was added during the reaction. Here, it is observed that the amplitudes of ultrasonic signals also increased with PDA content. Compared to the sensor with uncoated MWCNTs, an increase of 40% was obtained by the sensor with PDA15%@MWCNT. This implies that PDA coating has a positive effect on the changes in electrical resistance of the nanocomposite sensors under high-frequency micro-vibrations. With the addition of nanofillers, the conductive network inside the material would be more filled by the contact points between nanofillers. Although the PDA coating on the surfaces of MWCNTs would negatively affect electron transport, this elastic coating layer would enable MWCNTs to move closer to each other at the nanoscale but without making contact, leading to a stronger tunneling effect that is conducive to electron transport under micro-vibrations. At the same time, the highly viscous PDA would help the nanofillers to keep up with the movement of the PVDF substrates under high-frequency micro-vibrations, hence increasing of the amplitudes of the ultrasonic signals that were output.

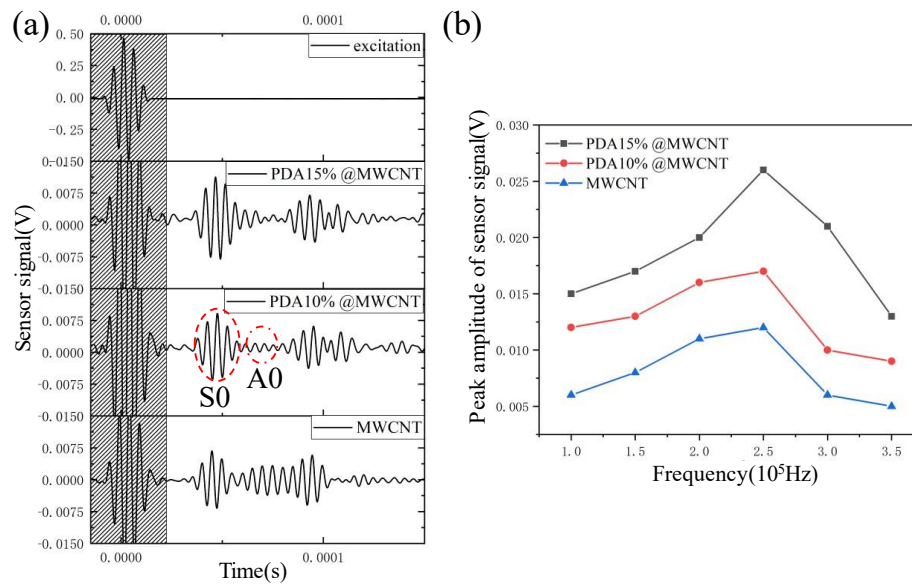


Figure 4. (a) The ultrasonic signals that were captured by nanocomposite sensors with uncoated MWCNTs and PDA@MWCNTs under an excitation frequency of 100 kHz (the shaded parts refer to either the excitation signal or cross-talks). (b) The peak amplitudes of the ultrasonic signals that were captured by nanocomposite sensors with uncoated MWCNTs and PDA@MWCNTs under various excitation frequencies.

Further, we observed the peak amplitudes of the ultrasonic signals that were acquired, at different excitation frequencies, by PDA@MWCNT nanocomposite sensors with different PDA loadings, as shown in **Fig. 4(b)**. Since the resonance frequency of the piezoelectric wafer that was used to excite ultrasonic waves is at 250 kHz, the peak amplitudes of the ultrasonic signals that were acquired by each of the nanocomposite sensors reach the maximum at 250 kHz. It is seen from the result that the nanocomposite sensor with a higher PDA coating level always demonstrates a higher sensitivity regardless of excitation frequency. This shows that the viscous PDA buffer layer is able to effectively transmit micro-vibrations from PVDF substrates to nanofillers over a very wide frequency range.

3.3.Characterization of nanocomposite sensors with hybrid nanofillers

Generally speaking, due to their long aspect ratio and high electrical conductivity, CNTs exhibit satisfactory rates of change in electrical resistance under relatively large strains. However, when receiving the microscopic strains (between 10s and 100s of nanometers) that are generated by ultrasonic waves, although the sensitivity of MWCNTs had been improved by PDA coating in this work, it still would not meet the requirement of real-world applications. This could be due to the high electron transport capacity of MWCNTs, and the lack of effective tunneling nodes which could be led to by the entanglement and the poor dispersion of the nanofillers^{57,58}. Under micro-vibrations, the change in electrical resistance of a sensor would be small, leading to a weak electrical voltage signal. Based on previous research work and theoretical analysis⁵⁹, it was found that single-layer graphene has a better capability in receiving ultrasonic wave signals. In this work, a nanocomposite material with hybrid nanofillers is proposed. By stacking one-dimensional MWCNTs and two-dimensional planar graphene, it would be possible to give rise to a larger number of effective tunneling nodes within a unit volume.

The dispersion of hybrid nanofillers in polymer substrates is useful to understanding the behavior of nanocomposite strain sensors under micro-vibrations. **Fig. 5(a)** and **(b)** show the SEM images of PDA@MWCNT/graphene hybrid nanofillers. It can be seen that the two different types of nanofillers were stacked together in the form of tablets and sticks, tightly combined with the PVDF substrate, and exhibited a good dispersion. MWCNTs were interspersed with graphene and the PVDF substrate, giving rise to a conductive network that would be more responsive to micro-vibrations. Since the SEM images could only reveal the cross sections of sensor films, TEM images were obtained to further uncover the stacking patterns of the hybrid nanofillers. The size and the morphology of the graphene used can be inferred from **Fig. 5(c)** and **(d)**. Single-layer graphene with a thickness of 4-7 nm presented a

zigzag border and had a large number of defects on the surface. At a larger magnification as shown in **Fig. 5(e)**, disordered stacking between the two types of nanofillers, which are of different dimensionalities, can be observed. In general, there are three ways in which the hybrid nanofillers could be stacked inside the proposed sensor: the contact between stick-shaped MWCNTs (as shown in **Fig. S2(a) and (d)**), the contact between graphene sheets (as shown in **Fig. S2(c) and (e)**), and the stacking of stick-shaped MWCNTs and planar graphene (as shown in **Fig. S2(g)**). It naturally follows that this cooperative stacking pattern can result in a larger number of effective tunneling nodes within a unit volume. The ratio between the occurrences of the three stacking modes would vary with the mass ratio between the two types of nanofillers. By changing the mass ratio between the hybrid nanofillers, it would be possible to explore the importance of each of the stacking modes to the performance of the proposed nanocomposite sensor.

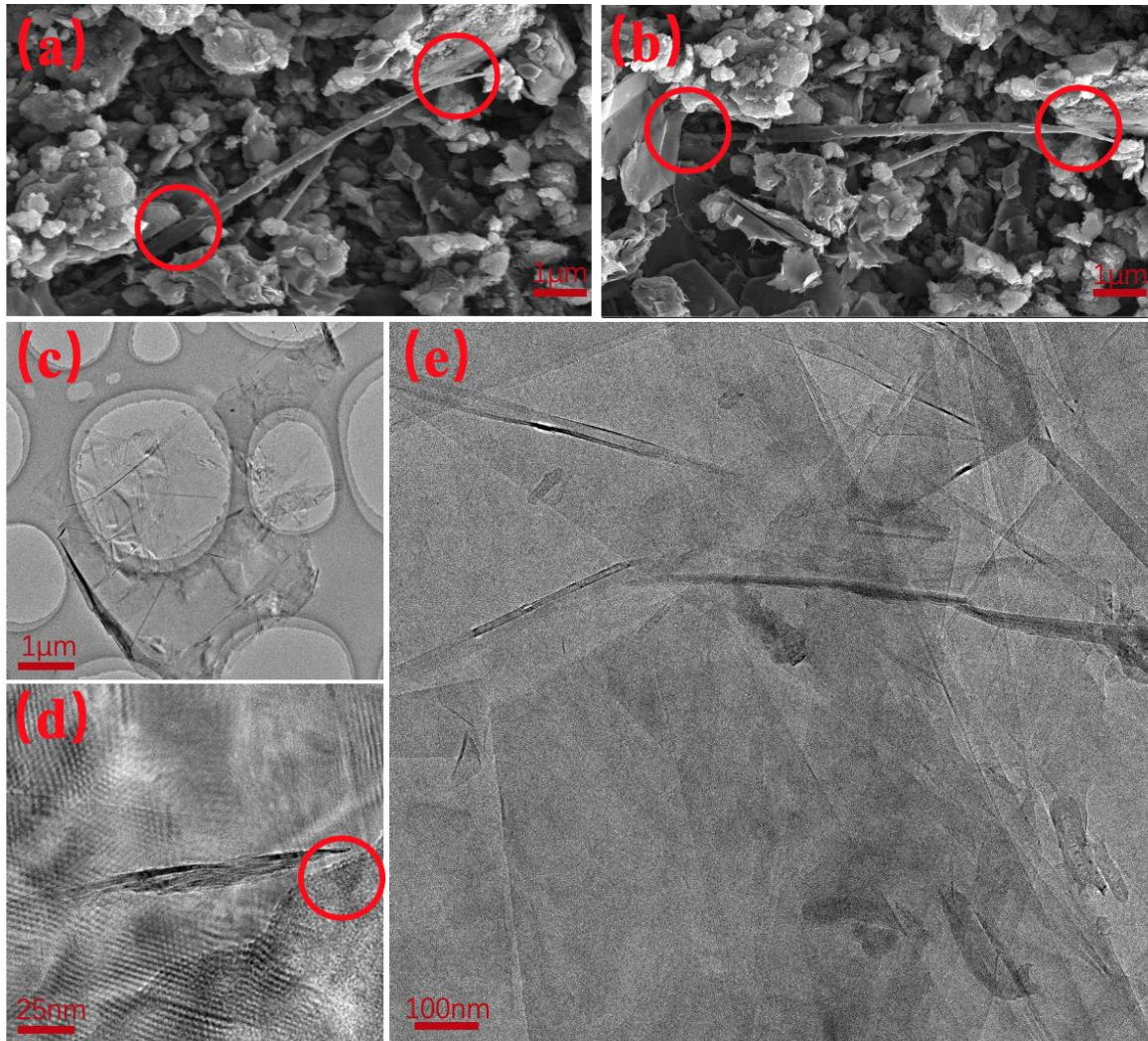


Figure 5. (a)-(b) The SEM images and (c)-(e) the TEM images of a nanocomposite sensor with hybrid nanofillers.

Fig. 6(a) shows the Raman spectra of nanocomposite strain sensors with hybrid nanofillers mixed at different mass ratios. Three peaks were observed, namely a D peak at $\sim 1355 \text{ cm}^{-1}$, a G peak at $\sim 1586 \text{ cm}^{-1}$ and a 2D peak at $\sim 2670 \text{ cm}^{-1}$. The first peak indicates a structural defect due to structural edge effects, while the second peak indicates the tangential vibrational mode of carbon atoms in the graphite structure. For a nanocomposite sensor, a high intensity ratio between the D and the G peaks (I_D / I_G) calculated from the Raman spectrum would correspond to a large number of inherent microstructural defects in the sensor, indicating a low local conductivity that is not conducive to electron movement. On the one hand, an

extremely low I_D / I_G would represent a high-density and saturated conductive network, in which case the tunneling effect between nanofillers would not be triggered when the sensor is subjected to external strains. It can be seen from the figure that with an increase in the mass fraction of graphene, the G peak rapidly increased, while the D peak remained at the original order of magnitude, meaning that the number of defects inside the material decreased and the remaining defects were largely attributed to the intrinsic defects of MWCNTs. Due to the geometric structure and the steric hindrance effect, the hybrid nanofillers can be effectively stacked on each other in a limited space to form a dense conductive network. However, it would be difficult for pure rod-shaped MWCNTs or flake graphene to form a perfect stacking.

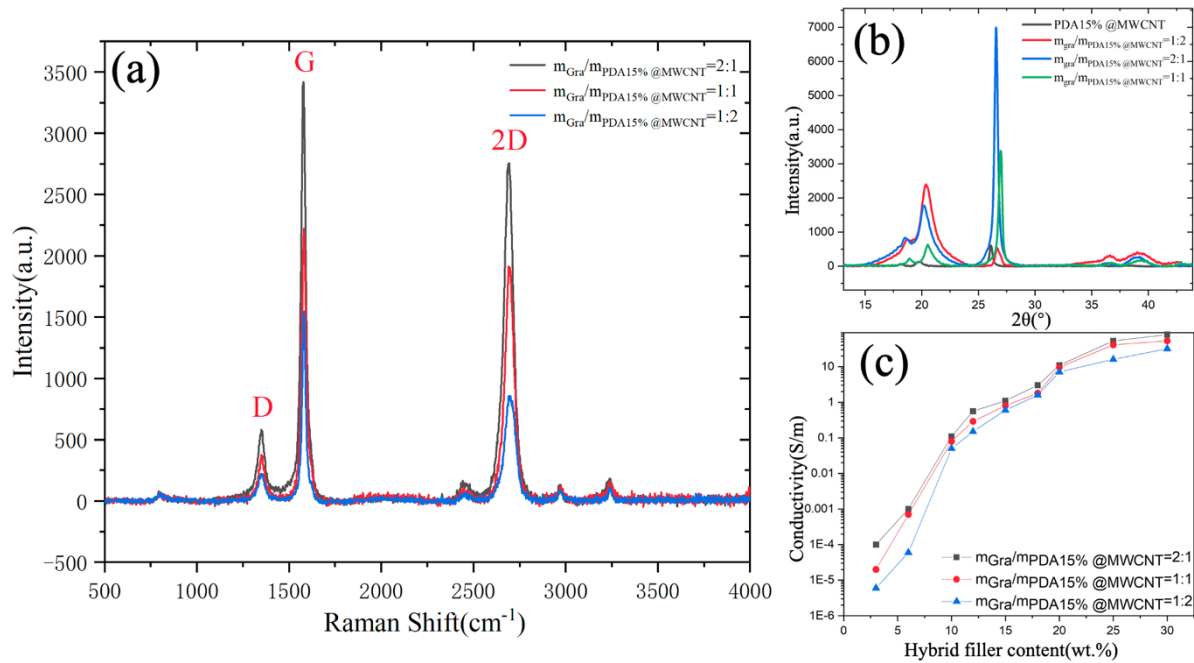


Figure 6. (a) The Raman spectra, (b) the XRD patterns and (c) the electrical conductivities of nanocomposite sensors with hybrid nanofillers mixed at different mass ratios.

The crystal morphologies of the sensors were further observed by XRD analysis. The XRD patterns, given in **Fig. 6(b)**, show that the diffraction peaks of the PVDF substrate at 2θ are 17.6° , 18.5° , 20.0° , and 26.6° , which correspond to the faces (100), (020), (100) and (021) of the α -phase crystal, respectively. This is related to the absence of heating during the synthesis

of the nanocomposite materials since the evaporation of the solvent at room temperature is conducive to the formation of α phase crystals of PVDF. From **Fig. 6(c)**, it can be seen that sensors with higher graphene contents possess slightly higher electrical conductivities, but the difference is within the same order of magnitude. Also, the conductivities of the sensors, which contain hybrid nanofiller mixed at different ratios, followed the same trend, meaning that the nanocomposite structures of the sensors had similar conductive paths and the slight differences in conductivity mainly originated from the variations in the geometrical contact between the hybrid nanofillers. Moreover, it is worth mentioning that the sensors with a hybrid nanofiller content of 15 wt.%, which were used for the subsequent assessment of the performance of the proposed nanocomposite sensor in acquiring ultrasonic waves, have a conductivity close to 1 S/m. Based on previous experimental research⁶⁰ and the characteristics of the inhouse bridge circuit / amplifier unit, it was found that sensor with a conductivity of 1 S/m would lead to the best performance in signal acquisition.

3.4. Performance of nanocomposite sensors with hybrid nanofillers in acquiring ultrasonic waves

Fig. 7(a) compares the ultrasonic signals that were acquired by nanocomposite sensors with hybrid nanofillers at different PDA coating levels. The excitation signal that was used is a 5-cycle Hanning-windowed sinusoidal toneburst with a central frequency of 200 kHz. It can be seen from the signals that the S_0 and the A_0 Lamb wave modes that propagated along the GFRP panel were faithfully captured. The positive effect of increasing the amount of PDA on the sensitivity of sensors, which was demonstrated and discussed in the previous section, remained qualitatively the same. However, quantitatively the effect of increasing the amount of PDA was much more significant for sensors with hybrid nanofillers, since the improvement that was brought about by using PDA15%@MWCNTs in the hybrid nanofillers over uncoated MWCNTs is as high as 180%. Owing to the fact that the graphene contents of the three sensors

are the same, it can be concluded that among the three types of contact modes of hybrid nanofillers, the stacking of graphene and MWCNTs has the most significant impact on the number of effective tunneling nodes.

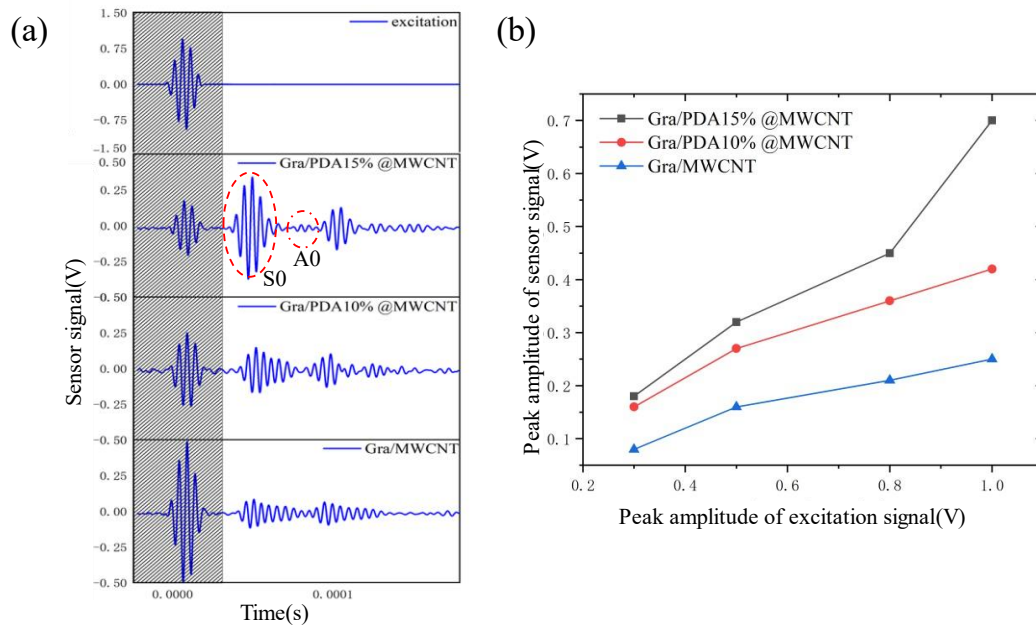


Figure 7. (a) The ultrasonic signals that were captured under an excitation frequency of 200 kHz by nanocomposite sensors with hybrid nanofillers with different PDA coating levels (the shaded parts refer to either the excitation signal or cross-talks). (b) The peak amplitudes of the ultrasonic signals that were acquired under various excitation voltages by nanocomposite sensors with hybrid nanofillers with different PDA coating levels.

In order to further evaluate the sensitivity of the nanocomposite sensors with hybrid nanofillers to ultrasonic waves, 5-cycle Hanning-windowed sinusoidal tonebursts with a central frequency of 200 kHz but different peak voltages were used to excite ultrasonic waves. As the peak excitation voltage was increased from 0.2 V to 1 V, the ultrasonic signals that were acquired became stronger, as shown in **Fig. S3**. **Fig. 7(b)** depicts the linear trends between the peak excitation voltages and the peak amplitudes of the ultrasonic signals that were acquired, proving that the proposed nanocomposite sensor is highly sensitive to ultrasonic waves, capable

of responding quantitatively to ultra-weak micro-vibrations. In addition, the slopes for sensors with higher levels of PDA coating are larger, meaning that the addition of PDA increases the sensitivities of sensors to ultrasonic waves. It further illustrates that the high sensitivity of the nanocomposite sensors with hybrid nanofillers was not just derived from graphene, which is known to be more sensitive than MWCNTs, but also the morphology and the structure of PDA@MWCNTs.

In order to illustrate the effect of graphene on the sensitivity of nanocomposite sensors with hybrid nanofillers, the ultrasonic waves that were acquired by nanocomposite sensors with hybrid nanofillers mixed at different ratios were examined, as shown in **Fig. 8(a)**. It can be seen that even the pure graphene nanocomposite sensor exhibits a far more superior sensitivity than the sensor that was made from uncoated MWCNTs. On the other hand, the sensitivity of the nanocomposite sensors with is on par with that of the pure graphene sensor. As the mass fraction of graphene in hybrid nanofillers was increased from 33% to 66%, the peak amplitude of the ultrasonic signals that were acquired by the sensors rose from 0.7 V to 1.5 V, exceeding the peak amplitude of the ultrasonic signal that was acquired by the pure graphene sensor. This shows that graphene plays an important role in determining the sensitivity the nanocomposite sensors with hybrid nanofillers.

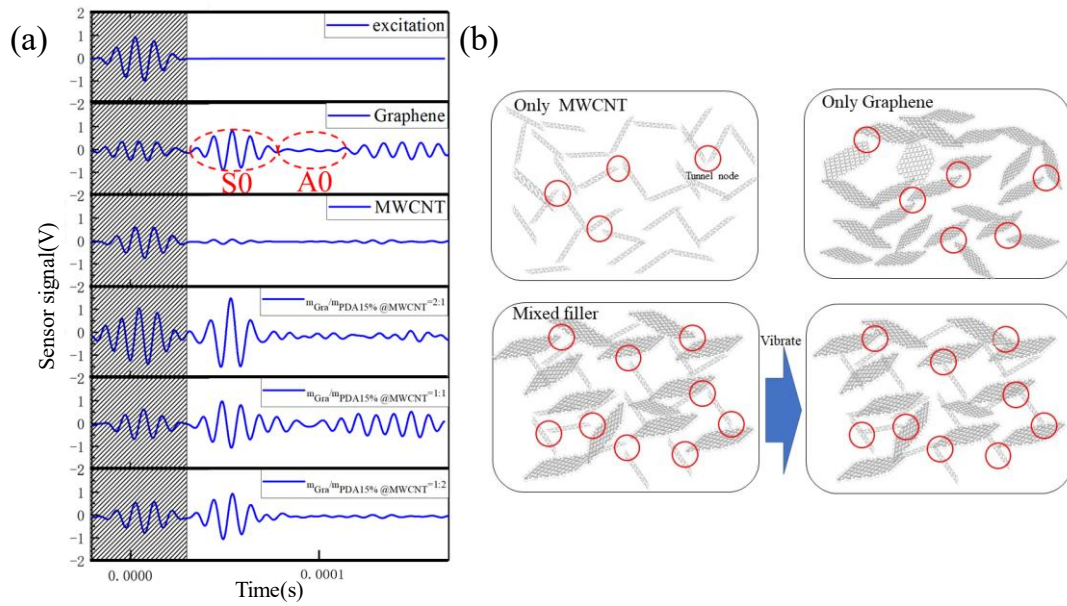


Figure 8. (a) The ultrasonic signals that were captured under an excitation frequency of 200kHz by a nanocomposite sensor that was made from uncoated MWCNTs, a pure graphene nanocomposite sensor, and nanocomposite sensors with hybrid filler mixed at different mass ratios (the shaded parts refer to either the excitation signal or cross-talks). (b) The schematic model of the stacking of the nanofillers in different types of nanocomposite sensors. The red circles highlight the possible contact modes of the nanofillers. In the nanocomposite sensors with hybrid nanofillers, the three type of contact modes are CNTs-CNTs, CNTs-Gra and Gra-Gra.

Based on the experimental results and the analysis that have been presented, it is shown that a nanocomposite strain sensor with hybrid nanofillers, which achieves a higher sensitivity than pure graphene sensors to the micro-vibrations that are generated by ultrasonic waves, has been successfully developed. The proposed sensor, which utilizes a lower graphene content, benefits from the synergy between the two different types of nanofillers which are of different dimensionalities, as shown in **Fig. 8(b)**. It would be difficult for pure MWCNT sensors or pure graphene sensors to gain sufficient tight and effective tunneling nodes due to poor stacking and

the steric hindrance effect which would be crucial to the acquisition of ultrasonic waves. Mixing nanofillers of two different dimensionalities can provide more ways for nanofillers to make contact with each other and increase the probability of forming tunneling nodes. Therefore, a higher sensitivity to ultrasonic waves was observed.

4. Conclusion

PDA coating was adopted and hybrid carbon nanofillers were used in this research to improve the sensitivity of nanocomposite strain sensors to ultrasonic waves. PDA@MWCNTs were analysed by XRD and XPS, and it was shown that PDA precipitated on the surfaces of the MWCNTs as single-crystal layers with a thickness of 10s nm. Through ultrasonic measurements over a wide range of frequencies, it was found that the thickness of PDA layers has a positive effect on the sensitivities of sensors. An improvement of approximately 40% was achieved over uncoated MWCNTs when the amount of PDA added was 15 wt.%. This indicates that PDA buffer layers positively influence tunneling processes because the tunneling effect is more likely to work only when the distances between conductive nanofillers are at the nanometer level. Nanocomposite sensors that were made from hybrid carbon nanofillers acquired ultrasonic signals at even more pronounced levels, demonstrating a sensitivity that is at least one order of magnitude higher than that of MWCNT based sensors. It was deduced that both types of nanofillers play an important role in improving the sensitivity of the proposed sensor, giving rise to enhanced geometrical contact between the nanofillers which intensified the tunneling effect. Also, as the mass fraction of graphene was increased from 33% to 66%, the sensitivity of the proposed sensor increased by approximately 120%. It surpasses that of pure graphene sensors, while a lower graphene content is used.

In summary, we put forward a new approach for optimizing the sensitivity of nanocomposite strain sensors to the micro-vibrations that are generated by ultrasonic waves.

The feasibility of the idea has been validated by a series of experiments that encompass both material characterizations and measurements of ultrasonic signals.

Acknowledgement

This work was supported by The Hong Kong Polytechnic University under Start-up Fund for New Recruits, the Research Grants Council of Hong Kong (grant no. 15204419), the Natural Science Foundation of China (grant no. 51875492 and 51627810), and the Ministry of Science and Technology of the People's Republic of China (grant no. 2018YFB502502-02).

References

1. Amjadi, M.; Kyung, K. U.; Park, I.; Sitti, M., Stretchable, Skin-Mountable, and Wearable Strain Sensors and Their Potential Applications: A Review. *Advanced Functional Materials* **2016**, *26* (11), 1678-1698.
2. Wang, X. W.; Liu, Z.; Zhang, T., Flexible Sensing Electronics for Wearable/Attachable Health Monitoring. *Small* **2017**, *13* (25).
3. Cai, G. F.; Wang, J. X.; Qian, K.; Chen, J. W.; Li, S. H.; Lee, P. S., Extremely Stretchable Strain Sensors Based on Conductive Self-Healing Dynamic Cross-Links Hydrogels for Human-Motion Detection. *Advanced Science* **2017**, *4* (2).
4. Liu, Q.; Chen, J.; Li, Y. R.; Shi, G. Q., High-Performance Strain Sensors with Fish-Scale-Like Graphene-Sensing Layers for Full-Range Detection of Human Motions. *Acs Nano* **2016**, *10* (8), 7901-7906.
5. Trung, T. Q.; Lee, N. E., Flexible and Stretchable Physical Sensor Integrated Platforms for Wearable Human-Activity Monitoring and Personal Healthcare. *Advanced Materials* **2016**, *28* (22), 4338-4372.

6. Wu, W., Stretchable electronics: functional materials, fabrication strategies and applications. *Science and Technology of Advanced Materials* **2019**, 20 (1), 187-224.
7. Liu, S.; Wang, Y.; Xu, W.; Leng, X. Q.; Wang, H. Z.; Guo, Y. N., et al. ,A novel sandwich-type electrochemical aptasensor based on GR-3D Au and aptamer-AuNPs-HRP for sensitive detection of oxytetracycline. *Biosensors & Bioelectronics* **2017**, 88, 181-187.
8. Pandey, S., Highly sensitive and selective chemiresistor gas/vapor sensors based on polyaniline nanocomposite: A comprehensive review. *Journal of Science-Advanced Materials and Devices* **2016**, 1 (4), 431-453.
9. N. Hu, T. Itoi, T. Akagi, T. Kojima, J. Xue, C. Yan, et al., Ultrasensitive strain sensors made from metal-coated carbon nanofiller/epoxy composites, *Carbon* 51 (C) (**2013**) 202e212.
10. Lee, B. M.; Loh, K. J., Carbon nanotube thin film strain sensors: comparison between experimental tests and numerical simulations. *Nanotechnology* **2017**, 28 (15).
11. Chen, J. K.; Wang, W. B.; Xuan, W. P.; Wang, X. Z.; Dong, S. R.; Garner, S., et al., Flexible surface acoustic wave broadband strain sensors based on ultra-thin flexible glass substrate. *Mrs Advances* **2016**, 1 (21), 1519-1524.
12. Han, M.; Kim, J. K.; Choi, Y. I.; Yun, J. P.; Lee, G. S.; Kang, S. W.; et al., Carbon nanotube-based strain sensor for structural health monitoring. *Japanese Journal of Applied Physics* **2019**, 58.
13. Lu, T. W.; Wu, C. C.; Lee, P. T., 1D photonic crystal strain sensors. *Acs Photonics* **2018**, 5 (7), 2767-2772.
14. Yoonessi, M.; Gaier, J. R.; Sahimi, M.; Daulton, T. L.; Kaner, R. B.; Meador, M. A., Fabrication of Graphene-Polyimide Nanocomposites with Superior Electrical Conductivity. *Acs Applied Materials & Interfaces* **2017**, 9 (49), 43230-43238.

15. Jafarzadeh, S.; Claesson, P. M.; Sundell, P. E.; Pan, J. S.; Thormann, E., Nanoscale Electrical and Mechanical Characteristics of Conductive Polyaniline Network in Polymer Composite Films. *Acs Applied Materials & Interfaces* **2014**, *6* (21), 19168-19175.
16. Wu, S. Y.; Ladani, R. B.; Zhang, J.; Ghorbani, K.; Zhang, X. H.; Mouritz, A. P.; et al., Strain Sensors with Adjustable Sensitivity by Tailoring the Microstructure of Graphene Aerogel/PDMS Nanocomposites. *Acs Applied Materials & Interfaces* **2016**, *8* (37), 24853-24861.
17. Zhou, C.; Su, Z. Q.; Cheng, L., Probability-based diagnostic imaging using hybrid features extracted from ultrasonic Lamb wave signals. *Smart Materials and Structures* **2011**, *20* (12).
18. Su, Z. Q.; Ye, L.; Lu, Y., Guided Lamb waves for identification of damage in composite structures: A review. *Journal of Sound and Vibration* **2006**, *295* (3-5), 753-780.
19. J. Sebastian, N. Schehl, M. Bouchard, M. Boehle, L. Li, A. Lagounov, et al., Health monitoring of structural composites with embedded carbon nanotube coated glass fiber sensors, *Carbon* **66** (C) (**2013**) 191.
20. Oh, T., The Tunneling Effect at Semiconductor Interfaces by Hall Measurement. *Korean Journal of Materials Research* **2019**, *29* (7), 408-411.
21. Liao, Y. Z.; Duan, F.; Zhang, H. T.; Lu, Y.; Zeng, Z. H.; Liu, M. L.; et al., Ultrafast response of spray-on nanocomposite piezoresistive sensors to broadband ultrasound. *Carbon* **2019**, *143*, 743-751.
22. Alamusi; Hu, N.; Fukunaga, H.; Atobe, S.; Liu, Y. L.; Li, J. H., Piezoresistive Strain Sensors Made from Carbon Nanotubes Based Polymer Nanocomposites. *Sensors* **2011**, *11* (11), 10691-10723.

23. Khodke, M. R.; Joshi, S. V., An investigative study on application of carbon nanotubes for strain sensing. *Nanosystems-Physics Chemistry Mathematics* **2016**, 7 (4), 755-758.
24. Liu, Y. D.; Kumar, S., Polymer/Carbon Nanotube Nano Composite Fibers-A Review. *Acs Applied Materials & Interfaces* **2014**, 6 (9), 6069-6087.
25. Khan, S. A.; Gao, M.; Zhu, Y. C.; Yan, Z. C.; Lin, Y., MWCNTs based flexible and stretchable strain sensors. *Journal of Semiconductors* **2017**, 38 (5).
26. Zhang, F.; Hu, H. L.; Islam, M.; Peng, S. H.; Wu, S. Y.; Lim, S.; et al., Multi-modal strain and temperature sensor by hybridizing reduced graphene oxide and PEDOT:PSS. *Composites Science and Technology* **2020**, 187.
27. Zhao, H.; Liu, X. J.; Chen, L. Z.; Chang, S. P.; Chang, M., Fabrication of ultra-high-sensitivity flexible strain sensor based on single ZnO nanowire. *Microsystem Technologies-Micro-and Nanosystems-Information Storage and Processing Systems* **2017**, 23 (6), 1703-1707.
28. Ramirez, J.; Rodriguez, D.; Urbina, A. D.; Cardenas, A. M.; Lipomi, D. J., Combining High Sensitivity and Dynamic Range: Wearable Thin-Film Composite Strain Sensors of Graphene, Ultrathin Palladium, and PEDOT:PSS. *Acs Applied Nano Materials* **2019**, 2 (4), 2222-2229.
29. Shintake, J.; Nagai, T.; Ogishima, K., Sensitivity Improvement of Highly Stretchable Capacitive Strain Sensors by Hierarchical Auxetic Structures. *Frontiers in Robotics and Ai* **2019**, 6.
30. Her, S. C.; Huang, C. Y., Thermal Strain Measured by Fiber Bragg Grating Sensors. *Sensors and Materials* **2016**, 28 (9), 939-946.
31. Balram, D.; Lian, K. Y.; Sebastian, N., Ultrasound-assisted synthesis of 3D flower-like zinc oxide decorated fMWCNTs for sensitive detection of toxic environmental pollutant 4-nitrophenol. *Ultrasonics Sonochemistry* **2020**, 60.

32. Ponnaiah, S. K.; Periakaruppan, P.; Muthupandian, S., Ultrasonic energy-assisted in-situ synthesis of Ru-0/PANI/g-C₃N₄ nanocomposite: Application for picomolar-level electrochemical detection of endocrine disruptor (Bisphenol-A) in humans and animals. *Ultrasonics Sonochemistry* **2019**, *58*.
33. Wei, P. P.; Shen, J.; Wu, K. B.; Yang, N. J., Defect-dependent electrochemistry of exfoliated graphene layers. *Carbon* **2019**, *154*, 125-131.
34. Bao, Y.; Tang, F. J.; Chen, Y. Z.; Meng, W. N.; Huang, Y.; Chen, G. D., Concrete pavement monitoring with PPP-BOTDA distributed strain and crack sensors. *Smart Structures and Systems* **2016**, *18* (3), 405-423.
35. Huang, Z. M.; Zhang, Y. Z.; Kotaki, M.; Ramakrishna, S., A review on polymer nanofibers by electrospinning and their applications in nanocomposites. *Composites Science and Technology* **2003**, *63* (15), 2223-2253.
36. Kwon, M. S.; Kang, D.; Kim, S.; Song, S.; Joo, C., Laser-speckle Strain Sensor using Structured Illumination. *Journal of the Korean Society for Nondestructive Testing* **2018**, *38* (5), 291-298.
37. Thostenson, E. T.; Ren, Z. F.; Chou, T. W., Advances in the science and technology of carbon nanotubes and their composites: a review. *Composites Science and Technology* **2001**, *61* (13), 1899-1912.
38. Chakraborty, D.; Nandi, U.; Dey, A. K.; Dasgupta, P.; Poddar, A.; Jana, D., Effect of Annealing Temperature on the Structural and the Electrical Transport Properties of La₂NiMnO₆ Nanoparticles. *Physica Status Solidi B-Basic Solid State Physics* **2018**, *255* (4).
39. Negishi, R.; Hasegawa, T.; Tanaka, H.; Terabe, K.; Ozawa, H.; Ogawa, T., Size-dependent single electron tunneling effect in Au nanoparticles. *Surface Science* **2007**, *601* (18), 3907-3911.

40. Robert, C.; Feller, J. F.; Castro, M., Sensing Skin for Strain Monitoring Made of PC-CNT Conductive Polymer Nanocomposite Sprayed Layer by Layer. *Acs Applied Materials & Interfaces* **2012**, *4* (7), 3508-3516.
41. Pandey, D.; Villani, M.; Colomes, E.; Zhan, Z.; Oriols, X., Implications of the Klein tunneling times on high frequency graphene devices using Bohmian trajectories. *Semiconductor Science and Technology* **2019**, *34* (3).
42. Tran, P. X., Modulation of Negative Differential Resistance in Graphene Field-Effect Transistors by Tuning the Contact Resistances. *Journal of Electronic Materials* **2018**, *47* (10), 5905-5912.
43. Hu, N.; Karube, Y.; Yan, C.; Masuda, Z.; Fukunaga, H., Tunneling effect in a polymer/carbon nanotube nanocomposite strain sensor. *Acta Materialia* **2008**, *56* (13), 2929-2936.
44. Obitayo, W.; Liu, T., A Review: Carbon Nanotube-Based Piezoresistive Strain Sensors. *Journal of Sensors* **2012**.
45. Kim, K. H.; Jang, N. S.; Ha, S. H.; Cho, J. H.; Kim, J. M., Highly Sensitive and Stretchable Resistive Strain Sensors Based on Microstructured Metal Nanowire/Elastomer Composite Films. *Small* **2018**, *14* (14).
46. Manna, K.; Wang, L.; Loh, K. J.; Chiang, W. H., Printed Strain Sensors Using Graphene Nanosheets Prepared by Water-Assisted Liquid Phase Exfoliation. *Advanced Materials Interfaces* **2019**, *6* (9).
47. Zheng, Y. J.; Li, Y. L.; Dai, K.; Wang, Y.; Zheng, G. Q.; Liu, C. T.; et al., A highly stretchable and stable strain sensor based on hybrid carbon nanofillers/polydimethylsiloxane conductive composites for large human motions monitoring. *Composites Science and Technology* **2018**, *156*, 276-286.

48. Ali, S.; Hassan, A.; Khan, S.; Bermak, A., Flexible coplanar waveguide strain sensor based on printed silver nanocomposites. *Sr Applied Sciences* **2019**, *1* (7).
49. Yoon, S. Y.; Kwon, I. B.; Yu, H. S.; Kim, E., Strain Transmission Ratio of a Distributed Optical Fiber Sensor with a Coating Layer. *Composites Research* **2018**, *31* (6), 429-434.
50. Li, X.; Li, Y.; Alam, M. M.; Chen, P.; Xia, R.; Wu, B.; et al., Enhanced thermal conductivity of nanocomposites with MOF-derived encapsulated magnetic oriented carbon nanotube-grafted graphene polyhedra. *Rsc Advances* **2020**, *10* (6), 3357-3365.
51. Yeom, Y. S.; Cho, K. Y.; Seo, H. Y.; Lee, J. S.; Im, D. H.; Nam, C. Y.; et al., Unprecedentedly high thermal conductivity of carbon/epoxy composites derived from parameter optimization studies. *Composites Science and Technology* **2020**, *186*.
52. Zhang, H. B.; Yan, Q.; Zheng, W. G.; He, Z. X.; Yu, Z. Z., Tough Graphene-Polymer Microcellular Foams for Electromagnetic Interference Shielding. *Acs Applied Materials & Interfaces* **2011**, *3* (3), 918-924.
53. Z. Su, L. Z., L. Qiu, H. Xu, Z. Zeng, M. Liu, Resistance-voltage transformation system for sensors in dynamic strain measurement and structural health monitoring. Patent, US 9,863,824B1 **2018**.
54. Lee, H.; Dellatore, S. M.; Miller, W. M.; Messersmith, P. B., Mussel-inspired surface chemistry for multifunctional coatings. *Science* **2007**, *318* (5849), 426-430.
55. Feng, Z. B.; Zuo, H. L.; Hu, J.; Gao, W. S.; Yu, B.; Ning, N. Y.; et al., Mussel-Inspired Highly Stretchable, Tough Nanocomposite Hydrogel with Self-Healable and Near-Infrared Actuated Performance. *Industrial & Engineering Chemistry Research* **2020**, *59* (1), 166-174.

56. Liu, Y. L.; Ai, K. L.; Lu, L. H., Polydopamine and Its Derivative Materials: Synthesis and Promising Applications in Energy, Environmental, and Biomedical Fields. *Chemical Reviews* **2014**, *114* (9), 5057-5115.
57. Costa, P.; Silva, J.; Anson-Casaos, A.; Martinez, M. T.; Abad, M. J.; Viana, J.; Lanceros-Mendez, S., Effect of carbon nanotube type and functionalization on the electrical, thermal, mechanical and electromechanical properties of carbon nanotube/styrene-butadiene-styrene composites for large strain sensor applications. *Composites Part B-Engineering* **2014**, *61*, 136-146.
58. Gibson, R. F.; Ayorinde, E. O.; Wen, Y. F., Vibrations of carbon nanotubes and their composites: A review. *Composites Science and Technology* **2007**, *67* (1), 1-28.
59. Duan, F.; Liao, Y. Z.; Zeng, Z. H.; Jin, H.; Zhou, L. M.; Zhang, Z.; et al., Graphene-based nanocomposite strain sensor response to ultrasonic guided waves. *Composites Science and Technology* **2019**, *174*, 42-49.
60. Zhou, P. Y.; Liao, Y. Z.; Li, Y. H.; Pan, D. Y.; Cao, W. X.; Yang, X. B.; et al., An inkjet-printed, flexible, ultra-broadband nanocomposite film sensor for in-situ acquisition of high-frequency dynamic strains. *Composites Part a-Applied Science and Manufacturing* **2019**, *125*, 10554.